C_{60} Fullerene Amphiphiles as Supramolecular Building Blocks for Organized and Well-Defined Nanoscale Objects

Yuming Zhao and Guang Chen

Abstract Fullerene-based nanomaterials have attracted extensive interest owing to their wide-ranging applications in materials science, nanotechnology, and biomedical research. This chapter gives an updated review of the recent advance in the design and characterization of fullerene derivatives as supramolecular building blocks for ordered and well-defined nanostructures and objects. The discussions are specially concentrated on the structural and morphological properties of discrete nano-aggregates by various amphiphilic fullerene derivatives formed in solution or at interfaces. Rationalization of the aggregation structure and morphology is attempted on the basis of amphiphilic molecular packing theories so as to shed light on the interplay between molecular factors (e.g., shape, polarity, non-covalent forces, and amphiphilicity) and self-assembly outcomes. Overall, this literature survey is aimed at mapping out applicable "bottom-up" strategies to control and preprogram the nanoscopic ordering of fullerene-based nanomaterials.

Keywords Amphiphile · Fullerene · Molecular packing · Nanomaterials · Self-assembly

Contents

Y. Zhao (✉) and G. Chen
Department of Chemistry, Memorial University of Newfoundland, St. John's, NL, Canada
A1B 3X7
e-mail: yuming@mun.ca

1   Introduction

Fullerenes constitute a fascinating class of molecular building blocks for the synthesis and fabrication of advanced nanoscale materials and devices [1–3]. In particular, C_{60} buckminsterfullerene has found a wide range of applications in various fields of modern nano-science and technology, owing to its extremely small size (0.498 nm in radius), highly symmetrical (I_h) molecular shape, and very rich electronic properties in both the ground and excited states [4]. Prominent examples of utilizing fullerene-based materials in cutting-edge research and applications include plastic solar cells, artificial photosynthetic mimicking, photo-dynamic therapy, gene delivery, molecular electronics, and nanomachinery, to name a few.

Over the past two decades, the covalent chemistry of C_{60} has evolved enormously, empowering synthetic chemists nowadays to flexibly modify the C_{60} structure with a vast array of molecular attachments ranging from organic and inorganic functional groups to macromolecular (e.g., polymers and dendrimers) moieties [5, 6]. In the current literature of fullerene chemistry, the synthesis of new fullerene derivatives is still a continuous and mainstream undertaking [7]. Beyond the molecular level, the supramolecular chemistry of C_{60} has also captured considerable attention due to the preponderance of such knowledge in material, biological, and medicinal applications [8–11]. For instance, the microscopic phase segregation of C_{60} acceptor domains in the active layer of bulk heterojunction (BHJ) organic solar cells has been known to exert a key influence on the efficiency of solar energy conversion [12–18]. Water-soluble fullerene derivatives bearing cationic side chains aggregate to form supramolecular self-assemblies with DNA which effectively promote gene transfection in mammalian cells [19, 20]. Nano-aggregates of pristine C_{60} (nC_{60}) have found to exert a negative (cytotoxic) effect on cell viability and antibacterial activity [21–23] while some water-soluble C_{60} derivatives on the contrary show greatly reduced cytotoxicity or non-cytotoxicity [24].

This chapter summarizes the recent studies of well-defined C_{60} nanostructures and objects resulting from supramolecular self-assembly in solution or at interfaces. It should be noted that by no means the review herein is intended to be comprehensive and thorough due to the vastness of pertinent literature. Rather, the discussions will be specifically focused on experimentally observed supramolecular aggregation behaviors of various C_{60} derivatives and relevant theoretical rationalizations. Collectively, this literature survey provides an updated overview to facilitate

the fundamental understanding of sophisticated supramolecular self-assemblies of C$_{60}$-containing molecules and to guide further exploration in the preparation of controllable and preprogrammable C$_{60}$-based nanomaterials and nano-devices.

2 Molecular Packing of Amphiphiles

Structurally buckminsterfullerene (C$_{60}$) is made up of sixty sp^2 hybridized carbons in a rigid spherical (soccer ball) shape [5]. The extensive π-electron delocalization over the C$_{60}$ cage renders it chemical reactivities resembling electron-deficient arenes or alkenes [6]. In terms of physical characteristics, C$_{60}$ has a very large cohesive force and is prone to aggregate significantly in solutions or at interfaces through non-covalent interactions such as π-stacking and van der Waals attraction [25]. As such, the C$_{60}$ cage is strongly hydrophobic and virtually immiscible in water (2×10^{-24} mol/L) and many polar organic solvents (e.g., 1×10^{-6} mol/L in acetone) [25, 26]. By some special means (e.g., solvent exchange, sonication, extended mixing, or some combination of these techniques) C$_{60}$ can be effectively suspended in water forming stable colloids (nC$_{60}$), as the clustering of C$_{60}$ minimizes the thermodynamically disfavored C$_{60}$-solvent contact [27, 28]. A quantitative understanding of the aggregation behavior and deposition kinetics of C$_{60}$ particles in aqueous media was recently established by Chen and Elimelech [29]. On the other hand, the solubility of C$_{60}$ in water or common organic solvents can be dramatically improved when it is functionalized with soluble organic moieties.

Generally speaking, for synthetic fullerene derivatives with well-defined molecular structures, the molecular attachments show better solubility in common solvents than the C$_{60}$ core as a result of the practical requirements for synthesis, purification, and characterization. As such, many C$_{60}$ derivatives in the literature can be viewed *as amphiphiles* in which the C$_{60}$ cage is solvophobic, whereas the pendant organic group(s) is solvophilic in nature. The aggregation behavior of such kind of C$_{60}$ derivatives is therefore, to a large extent, regulated by the rules of amphiphilic molecular packing. Mother Nature often uses amphiphilic molecules or macromolecules as the building blocks to construct complex superstructures with various shapes and functionality, such as bones, tissues, and cell membranes. The self-organization of natural materials that eventually make life possible is actually dictated by the "codes" inherent in each individual building components, such as molecular shape, covalent bonding structure, and various non-covalent interactions effected by different functional groups the molecule bears. Inspired by Mother Nature, a large variety of supramolecular structures with unique properties and functionality have been designed and synthesized by chemists using synthetic compounds mimicking those amphiphiles observed in the natural world [30–32]. Indeed, understanding of supramolecular self-assembling behavior and mechanisms has become the centerpiece of current nano-science and technology.

Table 1 Relationship between amphiphile shape and predicted aggregate morphology

Shape of amphiphile	Packing parameter (P)	Aggregate morphology
Cone	<1/3	Spherical micelles
Truncated cone	1/3–1/2	Wormlike micelles
Cylinder	1/2–1	Bilayer vesicles
Inverted cone	>1	Inverted micelles

A major driving force for the self-assembly of amphiphilic molecules in the solution phase is the *solvophobic* effect [33]. For instance, it has been long discovered that natural or synthetic surfactants at the so-called critical aggregation concentration in water tend to organize themselves into regular micelles driven by the hydrophobic effect. Depending on the nature of the amphiphiles and experimental conditions, the aggregation morphologies vary substantially from simple spheres and tubes to complex helices, twisted ribbons, braids, and so on. Investigations on these self-assembled structures hence paved a rational way for the design and synthesis of functional materials and devices with precise control and regulation on the nanometer scale. To this end, however, development of theoretical models with strong predictive power in terms of the shape-structure relationship for amphiphile packing is highly valued. The past few decades have witnessed an evolution of theoretical methods accounting for amphiphilic molecular packing outcomes. Based on the principles of statistical thermodynamics, Israelachvili et al. devised a "critical packing parameter" (CPC) approach to predict the aggregate morphologies resulting from amphiphilic surfactant packing at equilibrium. In this model, the packing parameter (P) is defined as:

$$P = V/(l \times a) \tag{1}$$

where V is the volume of molecule, l is the length of molecule, and a is the mean cross-sectional surface of head group. Table 1 gives the correlation between the shape of amphiphile monomer and the predicted aggregate morphology according to the Israelachvili model.

Simple and straightforward as it is, the Israelachvili's method offers both qualitative insights and prediction in agreement with a wide range of experimental results, giving a long-lasting impact in the amphiphilic packing literature. Nevertheless, this packing rule still has limitations to be addressed. Tsonchev et al. in 2003 came out with an approach of geometric packing analysis in which amphiphiles when treated as "hard" cones or truncated cones are predicted to always favor packing into spherical micelles because of the higher packing fraction [34]. The Tsonchev's model cast a new light on amphiphilic molecular packing and is in contrast to the commonly held belief that truncated cones will form cylindrical micelles. Most recently, more computationally expensive methods utilizing molecular dynamics (MD) simulation have been exploited by several groups in order to satisfactorily rationalize the clustering of amphiphiles in small numbers as well

as to reveal atomistical details driven by directional interactions other than hydrophobicity, such as electrostatic interactions [35–37], and hydrogen bonding [38].

Although it is reasonable to state that material chemists have now been adequately armed with theoretical guides for preparation of defined and well-organized nanosystems through controllable amphiphilic molecular packing, the exploration and rationalization of fullerene-based amphiphiles within this context is still kind of lagging behind other types of amphiphiles. Previously, there have been several review articles dedicated to related topics [30, 39]. However, the detailed interplay between molecular factors (structure, shape, and non-covalent forces) and supramolecular aggregation properties appeared to be random and evasive from being unequivocally debunked, mainly due to the limited capability of experimental measurements. In the past few years, a significant progress in the synthesis of new amphiphilic C$_{60}$ derivatives and study of their self-assembling behavior has been made, broadening the literature database for a revisit of this topic. It is therefore our intention that the present review would serve an updated roadmap for the current pursuit of "bottom-up" controlled supramolecular synthesis of fullerene-based nanomaterials.

3 Nano-Aggregates Assembled by C$_{60}$ Amphiphiles Bearing Chain-Like Polar Appendages

To prepare C$_{60}$-based amphiphiles, a straightforward approach is to tether a highly polar and water-soluble (hydrophilic) group such as ammonium to the C$_{60}$ cage via a molecular chain (e.g., alkyl, oligoethylene glycol). In 1999, Tour and coworkers investigated the supramolecular assembling properties of a C$_{60}$-N,N-dimethylpyrrolidinium iodide (**1**, Fig. 1a) [40]. After adding benzene to a solution of **1** in dimethyl sulfoxide (DMSO) and water, the mixture was agitated to yield a fluorescent and hair-like material in the organic (benzene) layer. The microscopic structures of the aggregates of **1** obtained under these conditions were characterized by transmission electron microscopy (TEM) to show an ordered rod-like morphology with diameters of 14–120 nm and lengths of over 70 μm (Fig. 1b). The nanorods formation was found to be solvent and counterion dependent. On the other hand, treatment of the aqueous solution of **1** with sonication followed by filtration through a 0.45μM filter resulted in the formation of vesicles (Fig. 1c). TEM study showed that the vesicles had diameters of 10–70 nm and wall thickness of 3–6 nm. The simply modified C$_{60}$-derivative **1** gave a facile way for preparation and manipulation of C$_{60}$ nano-assemblies. In the molecular structure of **1**, the hydrophilic pyrrolidinium moiety closely positioned to the hydrophobic C$_{60}$ cage only partially reduces the C$_{60}$–C$_{60}$ aggregation. It is obvious that π-stacking together with ionic interactions form the driving forces for the nanoscopic ordering. In a simple approximation, the molecular shape of **1** can be treated as an ellipsoid. According to the simple amphiphile packing rule, it is a case that favors packing
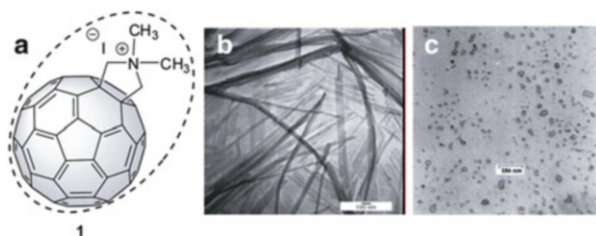
Fig. 1 (**a**) Structure of C_{60}-*N,N*-dimethylpyrrolidinium iodide **1**. (**b**) TEM image of nanorods of **1**. (**c**) TEM image of vesicular aggregates of **1** obtained after sonication and filtration. Adapted from [40] with permission. Copyright Wiley
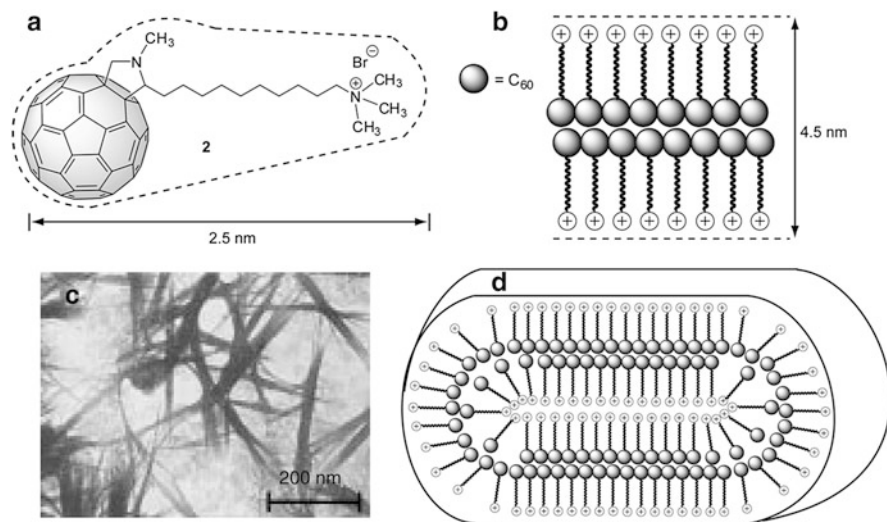

Fig. 2 (**a**) Structure of pyrrolidino-C_{60} amphiphile **2**. (**b**) Schematic drawing of molecular bilayer structure of **2**. (**c**) TEM image for an aqueous solution of **2**. (**d**) Schematic model for the disk-like aggregates of **2**. Adapted from [41] with permission. Copyright Wiley

into bilayer vesicles ($0.5 < P < 1$). Both of the observed morphologies, rods and vesicles, are kind of in line with the packing rule. However, a conclusive rationalization cannot be made in this case due to the lack of structural details in experimental measurements. Moreover, the two different assembling outcomes arising from different experimental conditions suggest that the aggregation of **1** is dependent on both thermodynamic and kinetic factors.

Nakashima and coworkers in 2002 prepared a similar pyrrolidino-C_{60} amphiphile **2** (Fig. 2a), in which a polar ammonium group was linked to C_{60} cage via a *n*-decylpyrrolidine chain [41]. Dispersed in an aqueous solution, C_{60}-amphiphile **2** was found to aggregate into fibrous and disk-like microstructures as evidenced by TEM imaging. X-ray diffraction analysis on the cast film of **2** revealed a *d* spacing from the Bragg's equation to be 4.33 and 4.46 nm before and after hot-water
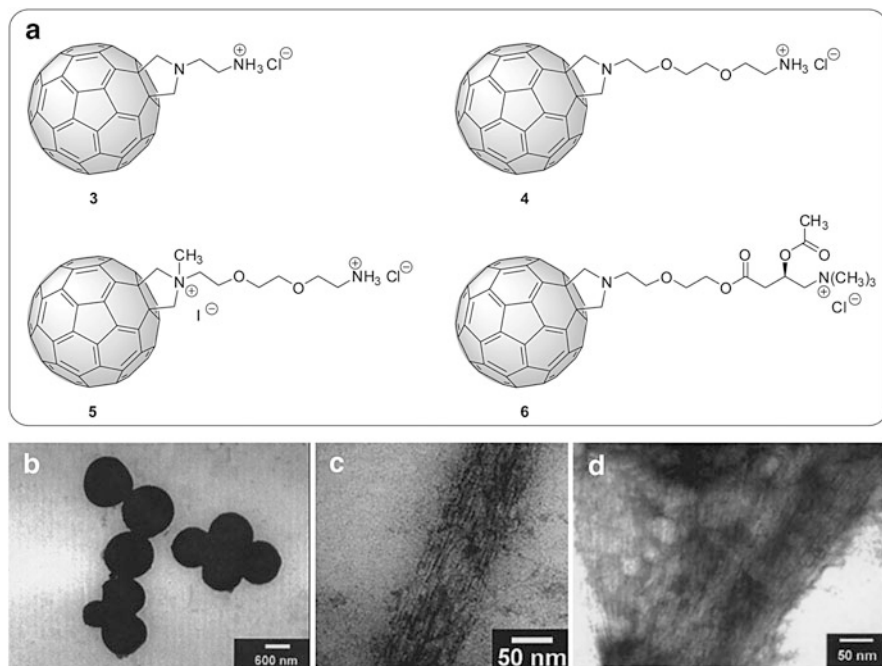
Fig. 3 (**a**) Structures of pyrrolidinofullerene amphiphiles **3–6**. (**b**) TEM image of spherical vesicles of **3**. (**c**) TEM image of a bundle of nanorods of **4**. (**d**) TEM image of a bundle of nanorods of **5**. Adapted from [42] with permission. Copyright PNAS

treatment. This result substantiated a hypothesis that the assembly was in a bilayer structure as illustrated in Fig. 2b. Furthermore, dynamic light scattering (DLS) study indicated that the particle size of the aggregates were in the range of 150–400 nm. A bilayer packing model (Fig. 2d) was proposed by the authors to account for the disk-like aggregation morphology. It is worth noting that sonication was also found to lead to molecular aggregates with smaller particle sizes (150–400 nm) in their experiments. Similar to Tour's C$_{60}$-amphiphile **1**, the molecular packing outcomes disclosed by Nakashima and coworkers present a case in accordance with the general amphiphile packing theory; that is, the rod-shaped amphiphile **2**, which can be viewed as a "cylinder," favors a bilayer packing structure at equilibrium (see Table 1). Nevertheless, the experimentally observed morphology showed a disk-like microstructure rather than vesicular assemblies is beyond the predictive scope of simple amphiphilic packing rules.

A series of pyrrolidinofullerene amphiphiles **3–5** (Fig. 3a) was investigated by Georgakilas and coworkers [42]. These amphiphiles are similar to the motif of **2** in that their structures are composed of a hydrophobic C$_{60}$ head and a hydrophilic quaternary ammonium tail. The tether groups connecting the two amphiphilic units in **3–5** were varied in both chain length and polarity (i.e., alkyl and oligoethylene glycol) to allow the effects of molecular structure to be probed. After dispersion in
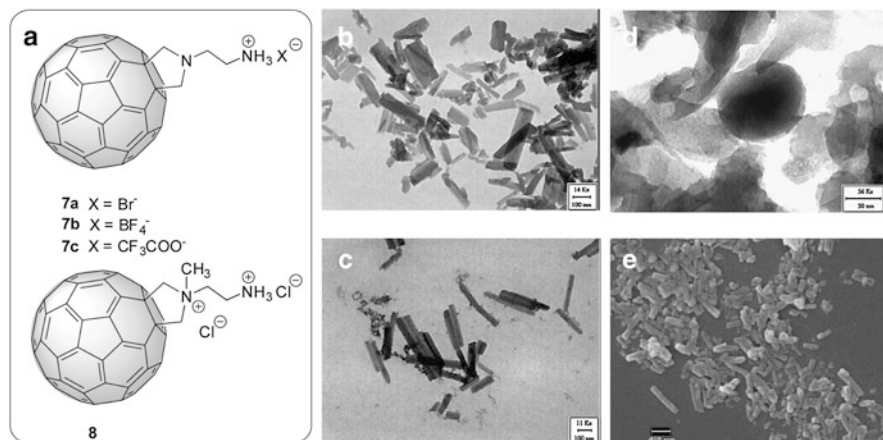
Fig. 4 (**a**) Structures of ammonium-attached pyrrolidinofullerenes **7a–c** and a doubly charged C_{60} amphiphile **8**. TEM images of nanorods of (**b**) **7a**, (**c**) **7b**, and (**d**) **7c**. (**e**) SEM image of **8** deposited on silicon substrate by spin-coating. Adapted from [44] with permission. Copyright Elsevier

water followed by sonication treatment, the relatively short and less polar amphiphile **3** was found to self-assemble into spherical vesicles with a dimension of 0.5–1.2 μM (Fig. 3b) as revealed by TEM study. When the tethering chain length was further elongated, however, a dramatic change in self-aggregation morphology was observed. As shown in Fig. 3c, d, long polar amphiphiles **4** and **5** exhibited a similar tendency to aggregate into long bundles of nanorods. Close inspection by TEM revealed that these bundled nanorods were uniformly aligned in a parallel manner. Computational modeling study suggested that a plausible molecular structure of the nanorods in which the hydrophobic C_{60} heads stacked inwardly in a fashion similar to C_{60}–C_{60} interactions occurring in the solid state. De Maria and coworkers prepared pyrrolidone-fullerene amphiphile **6** containing a chiral L-acetyl carnitine appendage (Fig. 3a) [43]. The molecule was found to form stable aggregates in water, and static light scattering analysis indicated that the sizes of the aggregated particles were in the range of 40–300 nm with an average size of 121 ± 44 nm. Due to the lack of microscopic investigation, the detailed structure and morphological properties of these nano-aggregates are still unclear, leaving the self-assembling behavior of chiral chain-like C_{60} amphiphiles an attractive topic awaiting further exploration.

In a general sense, the supramolecular assembling properties of chain-like C_{60} amphiphiles with ionic appendages are dictated by two major non-covalent forces, C_{60}–C_{60} π-stacking (attracting) and ionic interaction (repelling), while the exact morphological consequences appear to be primarily controlled by the delicate balance of these two interactions. Nevertheless, there are also other molecular and experimental factors that should not be overlooked. Prato and coworkers in 2006 demonstrated that the counterion plays a significant role in the self-organization of ammonium-attached pyrrolidinofullerenes **7** (Fig. 4) [44]. From
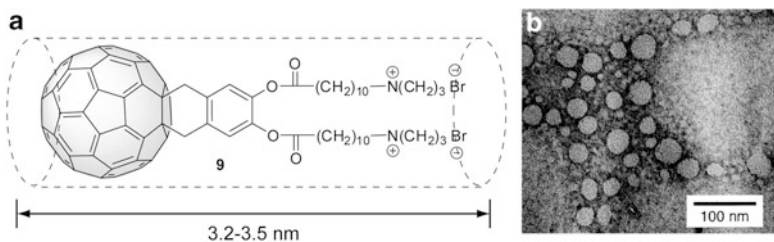
Fig. 5 (**a**) Structure of C$_{60}$ bolaphile **9**. (**b**) TEM image of dispersed vesicles of **9**. Adapted from [46] with permission. Copyright ACS

TEM imaging (Fig. 2b, c), C$_{60}$ amphiphiles associated with bromide (Br$^-$) and tetrafluoroborate (BF$_4^-$) anions were found, after sonication in water, to aggregate into ordered nanorods with lengths of hundreds of nanometers (80–500 nm for **7a** and 100–900 nm for **7b**) and widths of tens of nanometers (20–90 nm for **7a** and 50–70 nm for **7b**). Close-up examination of these nanorods revealed tube-like microstructures. When the counterion was switched to trifluoroacetate (CF$_3$COO$^-$), however, the resulting nano-agglomerates showed amorphous characteristics, clearly manifesting a prominent counterion effect. Scanning electron microscopic (SEM) and atomic force microscopic (AFM) characterizations were also performed on these C$_{60}$ aggregates, the results of which gave morphological properties in agreement with the TEM study. Moreover, a doubly charged C$_{60}$ amphiphile **8** was investigated, and it was found that the aggregates of **8** were structurally similar to those of **7a**, suggesting that the pyrrodinium moiety had little influence on the aggregation process. It should be noted that similar observation was also reported in the study of analogous amphiphiles (**4** and **5**) by Georgakilas [42].

Bola-amphiphiles or bolaphiles are molecules featuring a hydrophobic skeleton and two hydrophilic ends and have found appealing interfacial self-assembly properties mimicking the membranes of many organisms [45]. Sano and coworker reported a C$_{60}$ bolaphile **9** in 2000 (Fig. 5) [46]. With two water-soluble ammonium groups at the ends, this bolaphile self-assembled into spherical vesicles with diameters of 20–50 nm after sonication in water. Given the length of the molecule (ca. 3.2–3.5 nm) calculated by molecular modeling, the microstructure of these vesicles was proposed to be made of bilayers in which C$_{60}$ cores were packed in a head-to-head orientation. Such a bilayered vesicular assembling architecture is clearly in line with the general amphiphilic packing rules (Table 1) if one simply treats the molecular shape of C$_{60}$ bolaphile **9** as a "cylinder."

Self-organization of chain-like C$_{60}$ amphiphiles can be enhanced by introducing planar extended π-systems as ordering elements. For example, C$_{60}$ amphiphile **10** grafted with a porphyrin moiety was found to aggregate into uniform nanotubes with lengths of 500 nm and diameters of 30 nm (Fig. 6) [42]. Of note is that the nanotubular self-assemblies could only be obtained under the condition of sonication in water, implying that the process is kind of kinetically controlled. In principle, the molecular packing of **10** should be governed by three key π-stacking
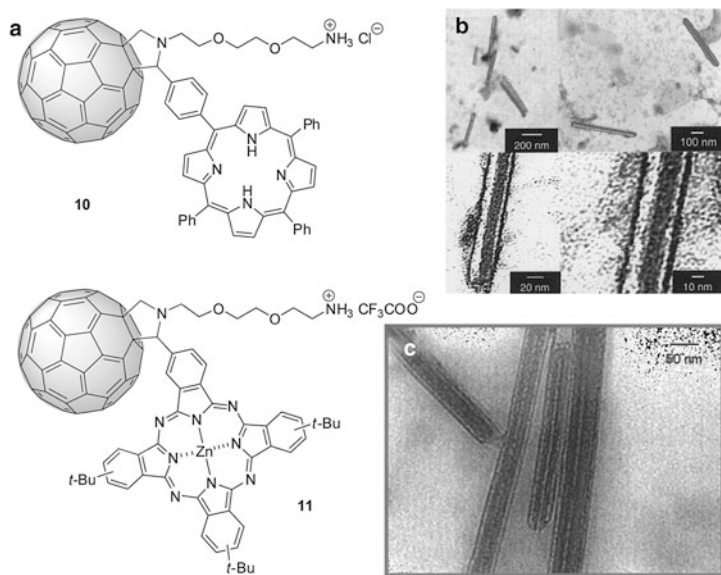
Fig. 6 (**a**) Structures of C_{60} amphiphiles **10** bearing a porphyrin appendage and **11** bearing a phthalocyanine appendage. (**b**) TEM images of nanotubes of **10** observed at different scales. (**c**) TEM image of nanotubes of **11**. Adapted from [42, 47] with permission. Copyright PNAS and ACS

driving forces: C_{60}–C_{60}, C_{60}-porphyrin, and porphyrin-porphyrin interactions. Modeling study suggested that porphyrin-porphyrin staking gave the most significant contribution to stabilizing the nanoscopic organization. An analogous C_{60}-amphiphile bearing a phthalocyanine (Pc) appendage (**11**, Fig. 6) was reported by Guldi and coworkers in 2005 [47]. Similar to **10**, amphiphile **11** also showed a strong tendency to form uniform nanotubes after dispersion in water by sonication. Photophysical studies indicated that nanostructured C_{60}-Pc assembly underwent ultrafast charge separation and ultraslow charge recombination, leading to an impressively long-lived charge-separation species [47]. These results suggested intriguing application of hybrid systems containing amphiphilic C_{60} skeletons and planar π-donors in organic photovoltaic devices. Given that π-stacking instead of geometric factors plays a dominant role in the supramolecular assemblies of **10** and **11**, simple amphiphilic packing rules do not provide any instructive insight into the morphological properties of their nano-aggregates. Obviously, more sophisticated theoretical modeling is required for better rationalization.

Recently, the aggregation behaviors of a series of pyrrolidino-C_{60} derivatives **12–16** (Fig. 7) carrying side chains with increasing hydrophobicity (from polar nonionic to polyionic) have been studies by De Maria and coworkers [48]. The hydrophobicity vs. hydrophilicity balance was evaluated by descriptors derived from aggregation measurements in aqueous/organic mixtures, partition measurements between *n*-octanol and water, and retention factors in reverse-
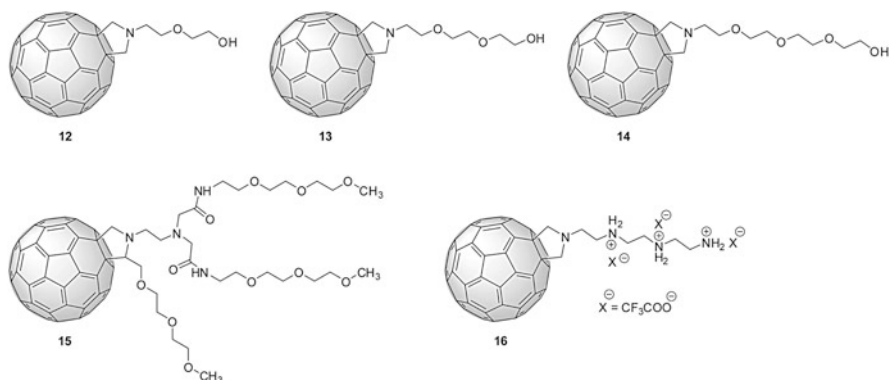
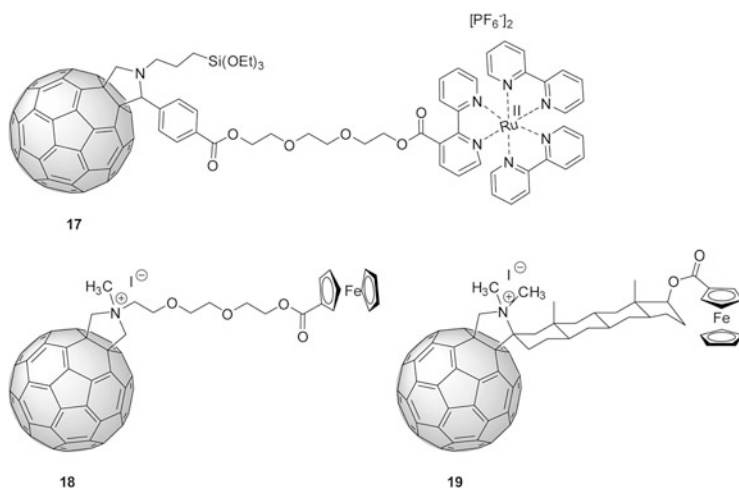Fig. 7 Structures of pyrrolidino-C$_{60}$ derivatives **12–16**

Fig. 8 Structures of C$_{60}$-Ru[bpy]$_3^{2+}$ hybrid **17** and fulleropyrrolidinium-ferrocene amphiphiles **18** and **19**

phase chromatography. TEM studies of the evaporation-induced aggregates of these C$_{60}$-amphiphiles showed nanometer-scale clusters with different sizes, and the detailed morphologies and structures were not so well defined to be rationalized or interpreted according to the general molecular packing theories.

Chain-like C$_{60}$ amphiphiles containing organometallic moieties have also been found to show ordered microscopic aggregating properties. For instance, the aggregates of C$_{60}$-Ru[bpy]$_3^{2+}$ hybrid **17** (Fig. 8) transferred from water to quartz surface formed microfibers made of nanosized clusters with diameters of ca.100 nm [49]. Substitution of the hydrophilic Ru[bpy]$_3^{2+}$ moiety of **17** with nonionic aromatic groups such as coumarin and fluorescein chromophores did not result in similar microstructures, underscoring the crucial role of Ru[bpy]$_3^{2+}$ in assembling

ordered supramolecular structures. Guldi and coworkers successfully used two fulleropyrrolidinium-ferrocene amphiphiles **18** and **19** to construct layer-by-layer (LBL) thin films, which assembled into linear nanowires [50]. The highly organized superstructures were believed to arise from complicated interplay between short- and long-range intermolecular interactions.

4 Nano-Aggregates Assembled by C_{60} Amphiphiles Bearing Branched or Dendritic Polar Appendages

Fullerene derivatives functionalized with multiple long side chains are usually very soluble in common organic solvents and even in water if water-soluble groups are embedded in the side chains. As such the supramolecular self-assembling properties are considerably altered in comparison to those relatively small and less soluble C_{60} amphiphiles. It was discovered in the late 1990s by several groups that attachment of multiple mesogenic units to the C_{60} core could give rise to interesting mesomorphic properties. For example, in 1996 Deschenaux and coworkers synthesized a C_{60} derivative **19** (Fig. 9), the structure of which contains two cholesterol moieties [51]. Compound **19** was the first example of C_{60}-based thermotropic liquid crystals. In the same year, Nakashima and coworkers reported an artificial fullerene lipid **20**, in which the side attachment is composed of three long alkyl chains (Fig. 9) [52]. Compound **20** shows solubility in common organic solvents, but is not water-soluble. Thin films of **20** were characterized by differential scanning calorimetric (DSC) analysis to show phase transition from crystalline to liquid crystalline phases. X-ray diffraction study suggested that **20** aggregated in a multilayered microstructure in the thin film. A large array of C_{60} derivatives in which a C_{60} core was linked to multiple mesogenic branches was prepared later, and their liquid crystalline properties were well summarized in a previous review [53]. Nevertheless, this class of C_{60} derivatives shows tendency to form good quality thin films rather than discrete particle-like aggregates. Such supramolecular assembling properties have been employed in the design of advanced C_{60}-based liquid crystalline materials in recent years [54–56].

A pyrrolidinofullerene **21** carrying a trialkoxybenzene appendage was synthesized by Nakanishi and coworkers in 2005 using the Prato method (Fig. 10) [57]. The supramolecular self-assemblies of **21** obtained after heating and aging in various solvents were examined by electron microscopy (SEM and TEM). It was found that the aggregate morphologies of **21** were solvent-dependent. In 2-propanol/toluene, spherical vesicles were formed with an average diameter of 250 nm (Fig. 10b). HR-TEM revealed that the vesicles take a two lamellae bilayer arrangement and the wall thickness was 8–9 nm. In 1-propanol, however, **21** aggregated into fiber-like microstructures and bundles of fibers with lengths greater than 20 μm (Fig. 10c). When 1,4-dioxane was employed as the solvent, the self-assemblies of **21** took the form of single bilayer discs (Fig. 10d). AFM imaging
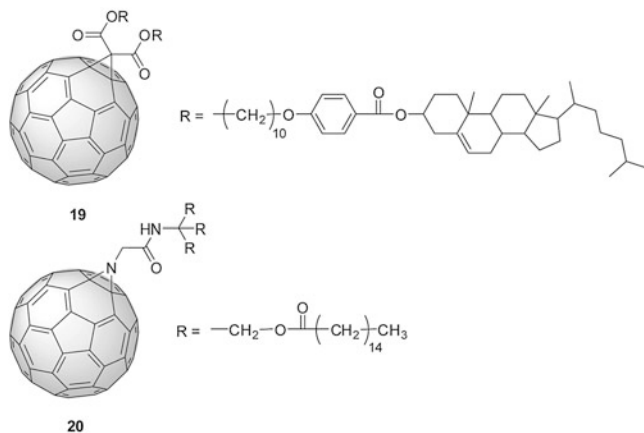
Fig. 9 Structures of C$_{60}$ derivative **19** with two cholesterol moieties and fullerene lipid **20** with three long alkyl chains
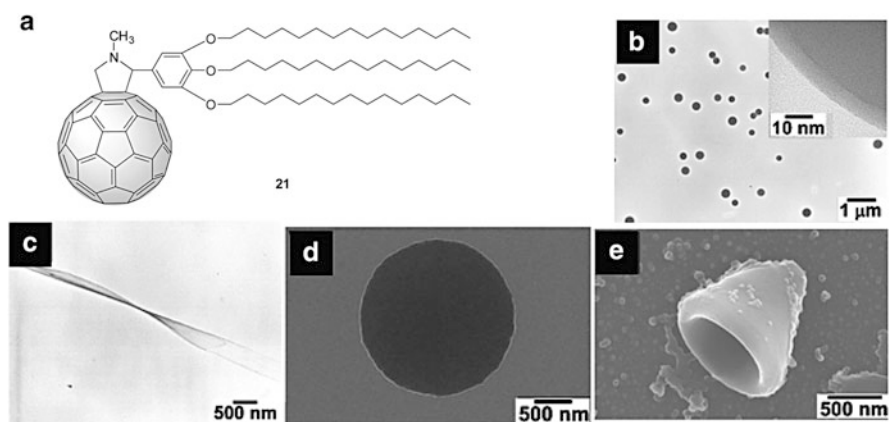

Fig. 10 (**a**) Structure of pyrrolidinofullerene **21** with a trialkoxybenzene appendage. (**b**) TEM and HR-TEM (*inset*) images of vesicles of **21** formed in 2-propanol/toluene. (**c**) SEM image of fiber-like aggregates of **21** formed in 1-propanol. (**d**) SEM image of single bilayer nanodisk of **21** formed in 1,4-dioxane. (**e**) SEM image of conical aggregate of **21** formed in 1:1 THF/H$_2$O. Adapted from [57] with permission. Copyright RSC

indicated that the discs had diameters of 0.2–1.5 μm and thickness of 4.4 nm. In 1:1 H$_2$O/THF, cone-shaped objects of submicron size together with disc-like structures were observed. The conical aggregate shown in Fig. 10e has a hole with a diameter of 60 nm, while the thickness of the shell is ca. 150 nm which corresponds to multilayer films. Thin films of **21** prepared by casting method were examined by XRD analysis to reveal an inter-fullerene distance of ca. 4.3 nm, suggesting the molecules were packed in an interdigitated bilayer architecture in the solid state.
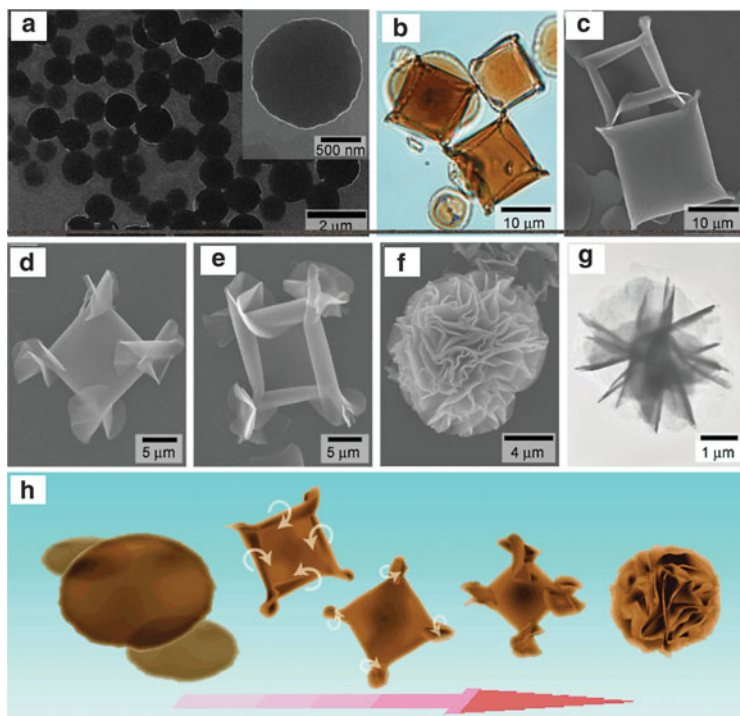
Fig. 11 Proposed mechanism for the formation of flower-shaped supramolecular assemblies of **21**. (**a**) SEM images of disk-shaped assemblies of **21** formed in 1,4-dioxane at 20°C as a precursor for the flower formation. (**b**) Optical microscopy and (**c**) SEM images of square-shaped objects loosely rolled up in every corner formed by rapid cooling of 1,4-dioxane solution of **21** from 60 to 5°C. (**d**), (**e**) SEM images of the further rolled-up objects of crumpled structures at the four corners. (**f**) SEM and (**g**) TEM images of the final flower-shaped objects formed by slow aging at 5°C. (**h**) Schematic representation of the formation mechanism of the flower-shaped supramolecular assembly. Reprinted from [58] with permission. Copyright Wiley

In 2007 Nakanish and coworkers prepared flower-shaped hierarchical supramolecular assemblies of **21** (Fig. 11f) under a sequence of preparation conditions: (1) heating in 1,4-dioxane to 60°C for 2 h; (2) aging at 20°C for 24 h; and (3) cooling to 5°C for at least 12 h [58]. The flower-like morphology had a dimension of 3–10 μm and was composed of sheet or flake-like nanostructures according to SEM and cryo-TEM studies. Variation of the preparation conditions allowed the intermediary morphologies to be observed, disclosing a transformation mechanism from flat bilayer disks, rolled up disks, to crumpled disks (Fig. 11). Moreover, spiral assemblies of **21** were prepared in different chiral butanols. The handedness of the spiral structure appeared to be originated from the hydrogen bonding interaction between **21** and the solvent molecules.

The supramolecular assemblies of a similar trialkoxybenzene-appended pyrrolidinofullerene **22** (Fig. 12a) was prepared by Nakanishi et al. in 2008
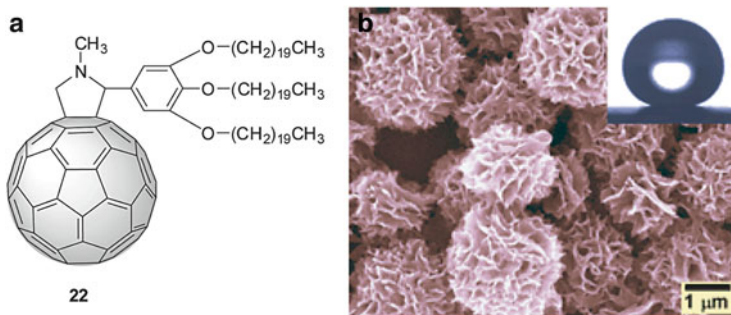
Fig. 12 (**a**) Structure of trialkoxybenzene-appended pyrrolidinofullerene **22**. (**b**) SEM image of globular objects of **22** deposited from a dilute 1,4-dioxane dispersion. Adapted [59] with permission. Copyright Wiley

[59]. The preparation conditions were as follows: heating the solution of **22** in 1,4-dioxane to 70°C and then cooling to 20°C. The resulting precipitates were analyzed by SEM and optical microscopy to show globular-shaped aggregates with diameters of a few microns and hierarchical organization of winkled flake-like submicron structures (Fig. 12b). HR-cryo-TEM analysis indicated these microstructures were assembled in the form of lamellar bilayer with a lamellar periodicity value of 4.4 nm. XRD analysis revealed a *d*-spacing value of 4.85 nm, which together with the TEM results suggested **22** packed in bilayer with the eicosyloxy chains interdigitated, given that **22** is about 3.6 nm in size. Of great interest is that thin films of **22** prepared on various substrates by slow evaporation method exhibited water-repellent superhydrophobicity with a water contact angle of ca. 152° (inset of Fig. 12b). SEM indicated that the thin films were ca. 20 nm in thickness and composed of densely packed globular aggregates (Fig. 12b). The superhydrophobicity arose from the fractal morphology of the two-tier roughness of both micro- and nanometer scale that mimics the leave's surface of lotus.

In 2010, Nakanishi and coworkers continued to prepare some supramolecular assemblies of trialkoxybenzene-pyrrolidinofullerenes associated with carbon nanotubes. It was discovered that the morphological changes of the aggregates of alkylated fullerenes could be used as a "temperature indicator" for photothermal conversion of carbon nanotubes (both single-walled and multiple-walled) in air upon near-infrared (NIR) laser irradiation [60]. This finding provided a useful approach to explore the photothermal properties of carbon nanotubes.

Dendrimers and dendrons are an appealing subclass of dendritic polymers and are commonly used as well-defined nano-building blocks owing to their predictable and controllable hierarchical structures and shapes [61–64]. In fullerene chemistry, the hybridization of C_{60} and various dendrimers has evolved into a fully fledged subtopic over the past decade [65, 66]. Arai and coworkers in 2006 reported a water-soluble C_{60} derivative **23** bearing a L-lysine dendrimer and two porphyrin units [67]. It was proposed that such a large molecule would show a globular-like structure in the solution phase. Dispersed in water, the molecules self-assembled
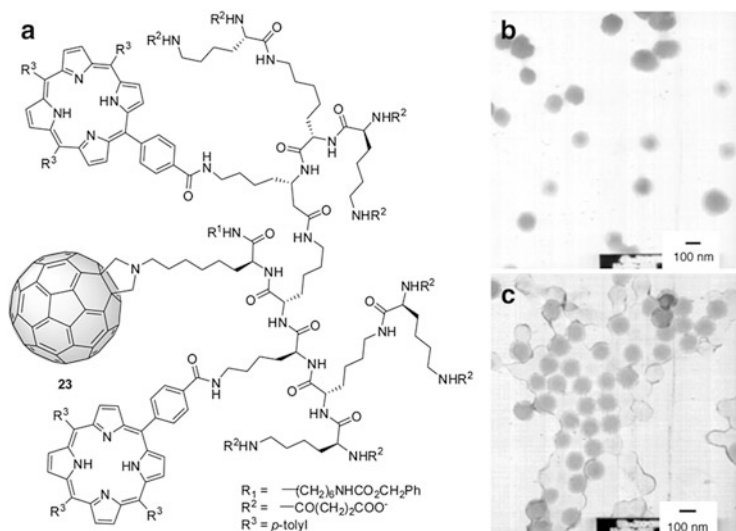
Fig. 13 (**a**) Structure of a water-soluble C_{60} derivative **23** bearing an L-lysine dendrimer and two porphyrin units. TEM image of samples cast from a solution of **23** in (**b**) H_2O ($\times 43,000$, 250 kV) and (**c**) 10 wt% 2-hydroxypropyl-β-cyclodextrin in H_2O ($\times 47,000$, 300 kV). Adapted from [67] with permission. Copyright ACS

into ordered nanospheres with the shape slightly distorted as revealed by TEM analysis (Fig. 13). The amphiphilicity and π–π interactions between fullerene and porphyrin units provided the driving forces for such an interesting supramolecular assembling behavior. The sizes of the aggregates of **23** in water were 90–170 nm determined by TEM. AFM study of the cast films of **23** on surfaces showed egg-shaped particles with sizes of 100–300 nm. Of particular interest is that when **23** was dispersed in water together with 2-hydroxypropyl-β-cyclodextrin (10%, wt), uniform spherical aggregates were observed by TEM, and the size distribution appeared to be much narrower (100–110 nm) compared with the case without cyclodextrin (Fig. 13c). It was reasoned by the authors that the addition of cyclodextrin tended to produce more homogeneous dispersion rather than causing de-aggregation. The spherical assemblies of **23** are in contrast to the regular nanotubes assembled by porphyrin-fullerene hybrids **11**. The extremely large globular molecular shape along with the complex hydrophilicity/hydrophobicity balance of **23** could be the reasons accounting for its unique self-aggregation properties in water.

In 2008, Martín and coworkers designed and synthesized a fullerene-dendrimer hybrid (dendrofullerene **24**, Fig. 14a), the structure of which consisted of a C_{60} core linked to a first-generation dendron and four π-extended tetrathiafulvalene (exTTF) peripheral groups [68]. Because of the favorable π–π interactions between convex C_{60} cage and the concave faces of exTTFs, dendrofullerene **24** was predicted to self-organize to form tree-like supramolecular assemblies (Fig. 14b). In a CHCl$_3$ solution of **24** (2.0×10^{-4} M), two sets of hydrodynamic radii were found by DLS
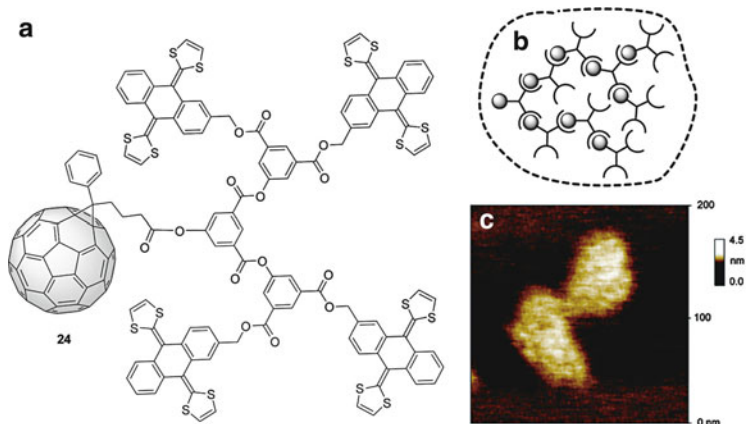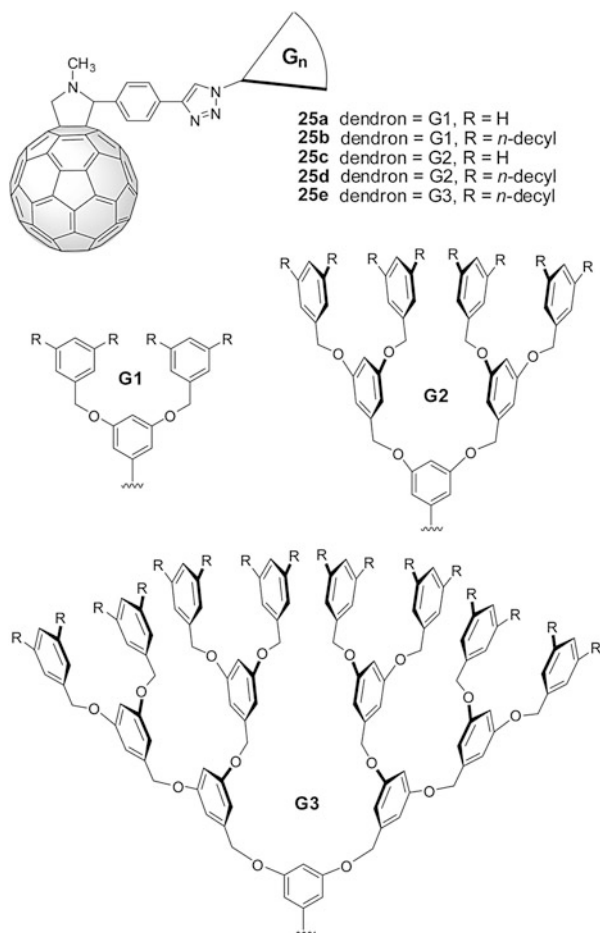
Fig. 14 (**a**) Structure of dendrofullerene **24** with four π-extended tetrathiafulvalene (exTTF) peripheral groups. (**b**) Self-assembly of **24** to form supramolecular dendrimer. (**c**) AFM image of a drop-cast of a CHCl$_3$ solution of **24** (10 μM) on mica. Adapted from [68] with permission. Copyright ACS

analysis, showing molecular clusters in the ranges of 5–15 nm and 0.78–1.0 μm, corresponding to monomeric to trimeric aggregates and multimetric associates, respectively. Aggregates prepared by drop casting on mica were imaged by AFM to show grape-like nanoparticles with uniform heights of 0.9–1.1 nm (Fig. 14c). A close inspection of the AFM image hints to that the large clusters were made up of small spherical aggregates grouped together by non-covalent π–π interactions. Although not conclusive about the details of the microstructure, the aggregation of **24**, if treated as a truncated cone in shape, seems to behave in line with the geometric packing model proposed by Tsonchev and coworkers [34].

Our group recently prepared a series of dendrofullerenes **25a–e** (Fig. 15) in which well-defined Fréchet-type dendrons ranging from the first to the third generations (G1 to G3) were connected to a pyrrolidinofullerene core through a Cu-catalyzed alkyne-azide cycloaddition (click reaction) [69]. The controllable molecular shapes of the dendron attachments render the dendrofullerenes a truncated cone-like structure, which accordingly would lead to spherical aggregates in amphiphilic molecular packing as schematically illustrated in Fig. 16a. Solvent (CHCl$_3$) evaporation-driven self-assemblies on exfoliated surfaces of mica were prepared by spin-coating method. AFM analysis revealed that the dendrofullerenes did not assemble into discrete nanoparticles with regular shapes but cross-linked worm-like aggregates or amorphous films. Such random interfacial self-assembly morphologies contradicted the amphiphilic packing rules and were ascribed to the weak amphiphilicity of dendrofullerenes **25**. To induce ordered supramolecular packing, acidification of the solution by trifluoroacetic acid (TFA) was conducted prior to spin-coating, as the protonation of the *N*-containing groups in dendrofullerenes **25** was expected to further enhance amphiphilicity. Indeed, this approach has been proven effective. Spherical nano-aggregates were observed in the thin

25a dendron = G1, R = H
25b dendron = G1, R = n-decyl
25c dendron = G2, R = H
25d dendron = G2, R = n-decyl
25e dendron = G3, R = n-decyl

films of **25** as evidenced by AFM imaging. Interestingly, the nature of the peripheral group appears to exert a significant control over the size of the nanospheres. In the case where phenyl groups constitute the outer surface of the dendron, very wide size distributions were found by statistical analysis of 100 nanoparticles in a selected region (4–44 nm for **25a** and 3–30 nm **25c**). Given the molecular spans of the two dendrofullerenes (ca. 2–3 nm according to CPK models), a significant portion of the nano-aggregates was believed to take multilayer micellar forms assembled through a C_{60}-phenyl stacking motif similar to that observed in the solid state [70].

Dendrofullerenes with n-decyl peripheral groups (**25b**, **25d**, and **25e**) were found to form uniform spherical nano-aggregates closely packed across the surface (Fig. 16d, e). Of great interest is the statistical analysis of the vertical height of nanoparticles revealed much narrower size distributions (Fig. 16b). From Table 2 it can be clearly seen that the theoretically predicted sizes of the monolayer nanospheres are consistent with the heights of particles measured by AFM, when
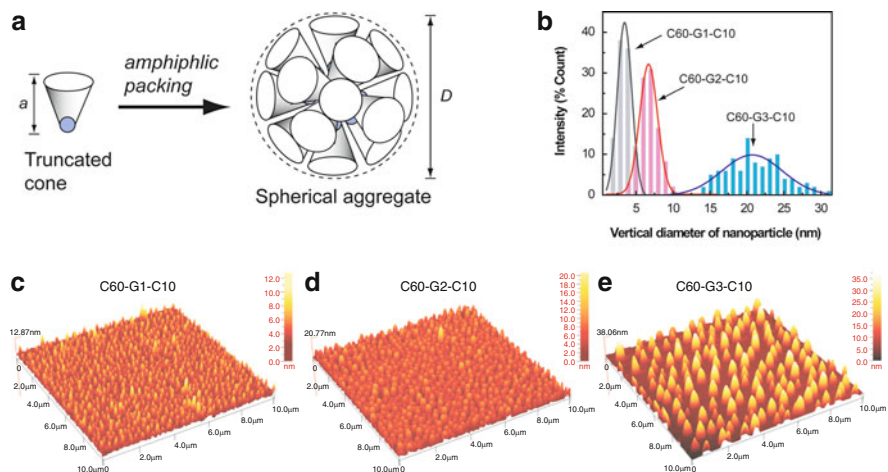
Fig. 16 (**a**) Spherical aggregation from truncated cones. (**b**) Statistical analysis of vertical diameters distribution for the spherical nano-assemblies of **25b**, **25d,** and **25e** prepared from spin-coating their dilute $CHCl_3$ solution on mica. AFM images of interfacial self-assemblies for (**c**) **25b**, (**d**) **25d**, and (**e**) **25e** under acidic conditions

Table 2 Relationship between amphiphile shape and predicted aggregated morphology

Entry	Length of amphiphile by CPK models (nm)	Predicted diameter of monolayer nanosphere (nm)	Average height of particles determined by AFM (nm)
25b	2	4	4.0
25d	4	8	7.2
25e	6	12	20.5

the dendrofullerene building blocks contained first- and second-generation dendrons. This result indicates that the *n*-decyl groups provide an effective insulating layer to prevent the monolayer nanospheres from further agglomeration. When the building blocks carried a third-generation dendron (**25e**), however, the predicted size of nanosphere is much smaller than the experimentally measured particle height. The discrepancy arises likely from the increased conformational flexibility of the larger dendron structure. Nevertheless, the use of dendrofullerenes bearing long alkyl peripheral groups has been demonstrated as an effective "bottom-up" means to attain uniform C_{60} nanospheres. As revealed by the analysis in Fig. 16b, narrowly distributed nanospheres can be produced via interfacial molecular packing. This work clearly shows that the shape and size of the nano-aggregates of C_{60} amphiphiles can be precisely controlled by systematically tuning the molecular structure as a dominating factor.

The Hirsch group recently reported the synthesis of a highly water-soluble dendrofullerene amphiphile **26**, the structure of which carries six nonionic, hydrophilic α-D-mannopyranosyl units as the peripheral groups (Fig. 17) [71]. This dendritic C_{60}-glycoconjugate showed a water solubility of >40 mg/mL and aggregated into small micellar sugar balls (nanospheres) in water of ca. 4 nm as
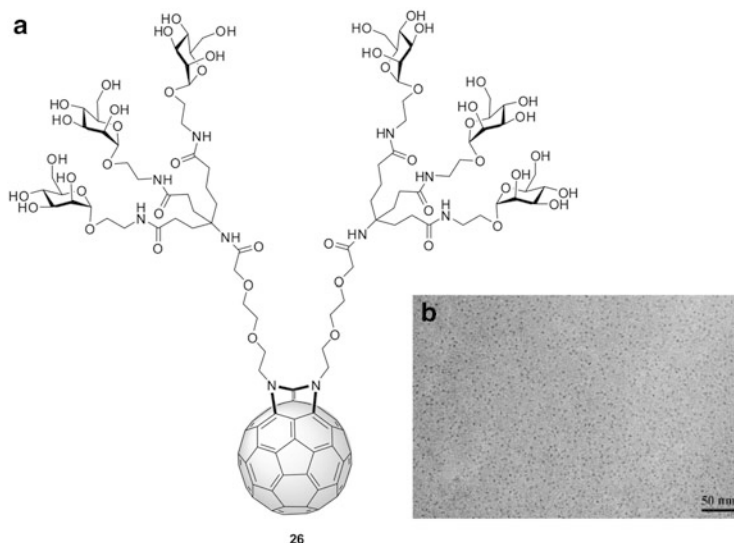
Fig. 17 (**a**) Structure of water-soluble dendrofullerene amphiphile **26** with six nonionic, hydrophilic α-D-mannopyranosyl units. (**b**) TEM image of the micellar sugar balls composed of **26**. Adapted from [71] with permission. Copyright Wiley

revealed by diffusion-ordered NMR and TEM studies. Given the truncated cone-like molecular shape of amphiphile **26**, the aggregation morphology is accountable based on the geometric packing theory as outlined by Tsonchev et al. [34].

Wang and coworkers reported the synthesis and supramolecular assembly of dendrofullerene **27** in 2010 [72]. The structure of this dendrofullerene consists of a hydrophobic C_{60} head, a hydrophilic poly(urethane amide) dendron (g_3-PUA), and a layer of hydrophobic *n*-hexadecyl peripheral groups (Fig. 18). The hydrogen bonding interaction within the g_3-PUA moiety renders the compound a flat plate-like molecular shape. In THF/H_2O (7:3, v/v) solution, dendrofullerene **27** self-assembled in an anisotropic manner to form ribbon-like aggregates as revealed by TEM imaging (Fig. 19b). AFM studies showed that the ribbons had thickness of 12.0 and 22.7 nm (Fig. 19a), corresponding to single- and double-layered structures as proposed in Fig. 19c, d. Moreover, small-angle X-ray scattering (SAXS) analysis of the ribbon-like aggregates suggested a lamellar structure with a *d* spacing of 9.24 nm. The value is smaller than the thickness found by AFM, suggesting an arrangement of interdigitated alkyl chains (Fig. 19d).

In addition to the dendrofullerenes, a class of "shuttle-coke" like penta-substituted fullerenes **28** (Fig. 20) is worthy of special remarks. This type of fullerene derivatives can be readily prepared through a fivefold organocopper addition to C_{60} developed by Nakamura and coworkers [70, 73–75]. Treatment of the compounds with a strong base, KO^{t}Bu, would lead to the formation of potassium fullerenide $[R_5C_{60}]^-K^+$ (R = aryl or alkyl) which can be solubilized in water with good stability. In contrast to many water-soluble fullerene derivatives, the
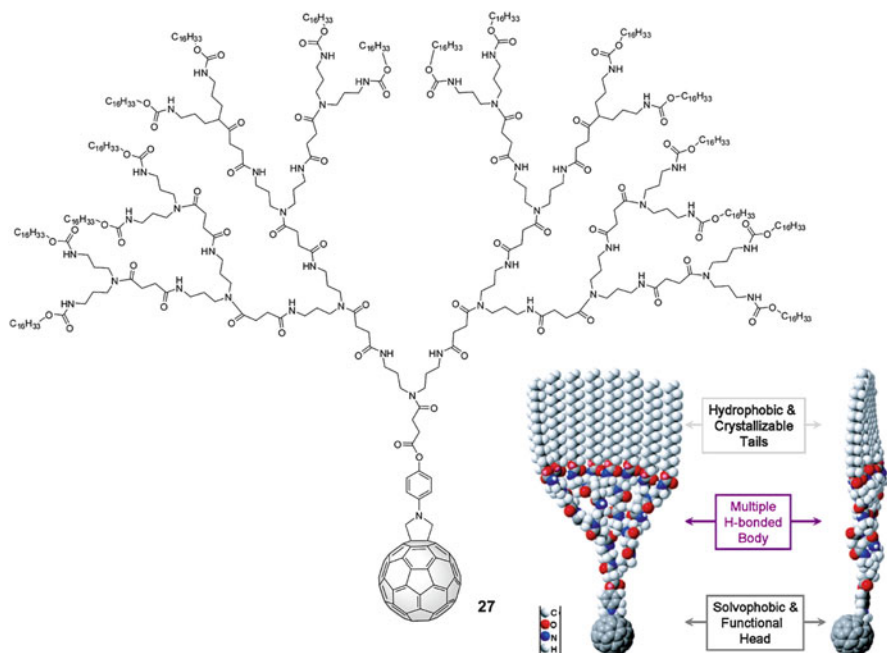
Fig. 18 Structure and molecular model of dendrofullerene **27**. Adapted from [72] with permission. Copyright ACS
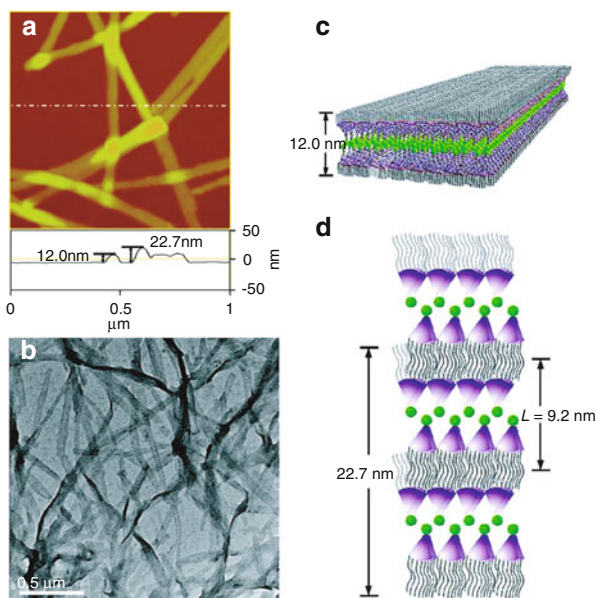

Fig. 19 (**a**) Tapping mode AFM image of aggregates of **27** formed in THF/H$_2$O (7:3, v/v) solution after spread on a silicon surface. (**b**) TEM image of ribbon-like aggregates of **27** formed in THF/H$_2$O (7:3, v/v) solution. Adapted from [72] with permission. Copyright ACS
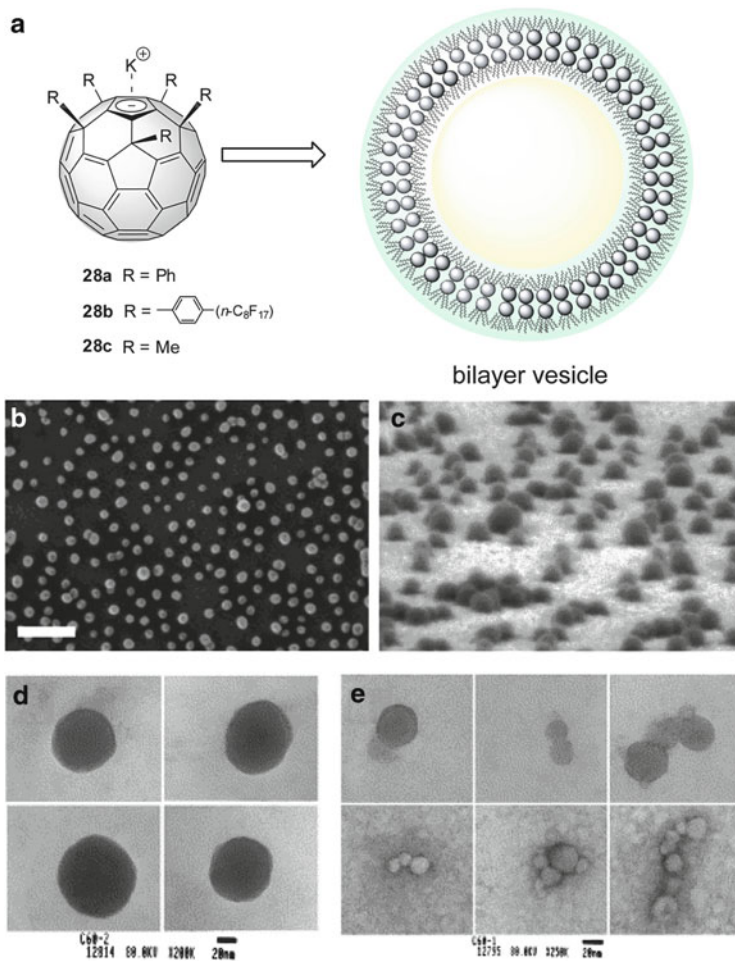
Fig. 20 (**a**) Structures of the penta-substituted fullerene potassium salts **28a–c** and their bilayer vesicle formation. (**b**) SEM image of vesicular **28b-**covered ITO surface. The scale bar represents 100 nm. (**c**) SEM image of a different area of the same vesicular **28b-**covered ITO sample viewed with 80° tilting of the sample stage. (**d**) TEM images of isolated vesicles of **28c**. (**e**) TEM images of isolated clusters of **28c**. Adapted from [78, 79] with permission. Copyright Wiley and Elsevier

$[R_5C_{60}]^-K^+$ type of compounds shows a reverse amphiphilic nature; that is, the hydrophilicity comes from the negatively charged C_{60} core, while the side-chain substituents are water repelling. Deposition of a dilute aqueous solution of the pentaphenyl fullerenide anion (**28a**) on mica resulted in globular particles as evidenced by AFM analysis [76]. The heights of the particles were 5–16 nm, which is in accordance to the results of DLS analysis (averaged apparent hydrodynamic radius 16.8 nm, polydispersity 0.18 ± 0.02) [76]. LLS analysis revealed that the self-assembled nanospheres of **28a** in water assumed a bilayer vesicular form as schematically illustrated in Fig. 20a [77]. The vesicles featured an average

hydrodynamic radius and radius of gyration of ca. 17 nm at a very low critical aggregation concentration ($<10^{-7}$ M). The average aggregation number of the associated particles was estimated to be about 12,000.

Recently, Nakamura and coworkers demonstrated that the pentaphenyl fullerenide anion bearing fluorous tails can give rise to organized supramolecular assemblies in water and on solid surfaces [78]. DSL analysis of **28b** in water indicated that stable bilayer vesicles were formed with a narrow size distribution and an average radius of 18.1 ± 0.1 nm. Spin-coating of **28b** on the indium tin oxide (ITO) substrate led to the formation of uniform vesicles. SEM studies showed that the vesicles were assembled on the ITO surface with a density of 228 ± 14 vesicles/μm^2 and an average radius of 17.8 ± 0.2 nm. It is also remarkable that unlike other lipid vesicles, the vesicles of **28b** assembled on surfaces showed very good structural integrity under vacuum. For instance, even at 10^{-5} Pa, spherical shape was retained for the nano-aggregates on ITO (Fig. 20b, c). Pentamethyl fullerenide anion **28c** under dilute conditions self-assembled into similar bilayer vesicles (Fig. 20d); however, the sizes of the vesicles (radius 27 nm and aggregation number 21,000) appeared to be considerably larger than those of **28a** and **28b**. The aggregates of **28c** formed above the critical reaggregation concentration (CRC) were clusters made of spherical vesicles in various sizes and geometries (Fig. 20e), suggesting a significant rearrangement of the anion surfactants and counterions [79].

5 Nano-Aggregates Assembled by Amphiphilic Hexakis Adducts of C_{60}

From the aforementioned examples, the strong π–π attraction between C_{60} cages appears to be a major driving force dictating the aggregation of C_{60} amphiphiles into a small-sized nanoparticle. In the case of heavily functionalized C_{60} derivatives, however, the C_{60} spheres are usually well shielded or encapsulated by the addend groups. As such, the C_{60} inter-cage interactions can be substantially reduced and its contribution to the aggregation behavior is negligible. Actually, such an effect has provided a useful approach for the preparation of ordered and reversible C_{60}-containing Langmuir or Langmuir–Blodgett (LB) thin films at the air-water interface [66, 80–85].

In 2005 the Hirsch group synthesized an amphiphilic [5:1]-hexakis adduct of C_{60} **29** (Fig. 21), in which two water-soluble dendrons were connected to the C_{60} core by amide linkers [86]. This amphiphile was found to show aggregation properties dependent on the pH of media. In neutral water (pH 7.2), compound **29** aggregated into mostly cylinders with a diameter of ca. 65 nm as revealed by cryogenic TEM studies (Fig. 22a). The tubular aggregates were reconstructed base on dimensions and density profile, suggesting a double-layered self-assembly motif in which roughly eight molecules occupied in the circular cross-section area (Fig. 22b).
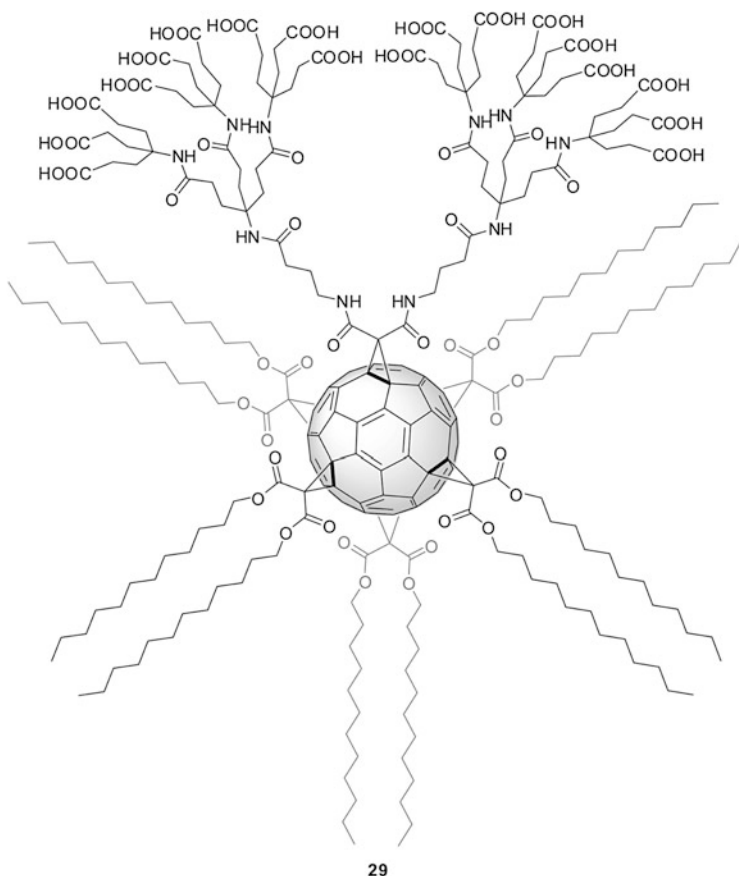
Fig. 21 Structure of amphiphilic [5:1]-hexakis adduct of C_{60} **29** with two water-soluble dendrons

When the pH of the solution was increased to 9.2, exclusive formation of structurally defined micellar spheres was observed (Fig. 22c) with a diameter of ca. 8.5 nm. The 3D organization of these spherical aggregates was determined by a simulation method to possess a C_2-symmetrical cubic arrangement composed of eight molecules oriented in such a way that all the hydrophobic parts of the molecules were efficiently shielded by the hydrophilic groups from the aqueous environment (Fig. 22d). The pH-dependent aggregation behavior was attributed to the different degree of protonation that altered the repulsion and the size of hydration shell. Also of note is that when the amide linker groups of **29** were switched to esters, the aggregation morphologies differed dramatically; bilayer sheets or liposomes became the predominant structures [87]. An explanation for this is that the dendritic amide moieties in **29** have more pronounced rigidity that favors aggregation with a high degree of curvature rather than a planar alignment [86].
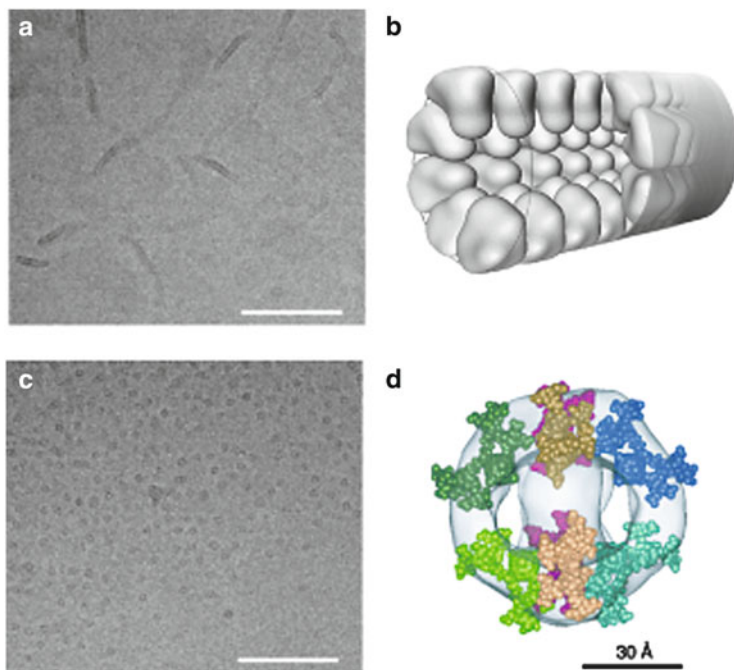
Fig. 22 (**a**) TEM image of rod-shaped double-layer aggregation of **29** at pH 7.2. (**b**) Proposed model of a molecular arrangement of **29** in micellar rods at neutral pH. The employed head-group volume is based on the partly protonated form. Hydrophobic alkyl chains, which should reside at the center of the micelle, are not shown for clarity. (**c**) TEM image of globular micelles formation of **29** at pH 9.2. (**d**) Eight head groups of the dendritic fullerene molecule may be fitted in a C$_2$-symmetrical mode into the reconstructed electron-density map. Reprinted from [86] with permission. Copyright Wiley

To understand the factors that dictate the structural persistence, Hirsch and coworkers further designed and investigated a [3:3]-hexakis C$_{60}$ adduct **30** in 2007 (Fig. 23a) [88]. Unlike amphiphile **29**, compound **30** carries three hydrophilic G-1 dendrons, with each dendritic branch ended with nine carboxyl groups. Although the total number of carboxyl functionalities was identical to that of amphiphile **29**, the space occupied by the hydrophobic moieties was much reduced. TEM analysis of the aggregates of **30** in water by a negative-staining technique disclosed the formation of uniform nanospheres with a diameter of ca. 5 nm (Fig. 23b). 3D reconstruction based on molecular modeling and TEM imaging indicated that these spherical micelles were made of three identical *S*-shaped motifs in the D_3 symmetry (Fig. 23c). It was also found that each *S*-shaped segment consists of two molecules of **30**. Overall, the spheres were assembled to minimize the contact of the hydrophobic cores with the water surrounding. The hexakis adducts of C$_{60}$ demonstrated by Hirsch and coworkers have not only provided insight into the precise nanoscopic organization of the supramolecular
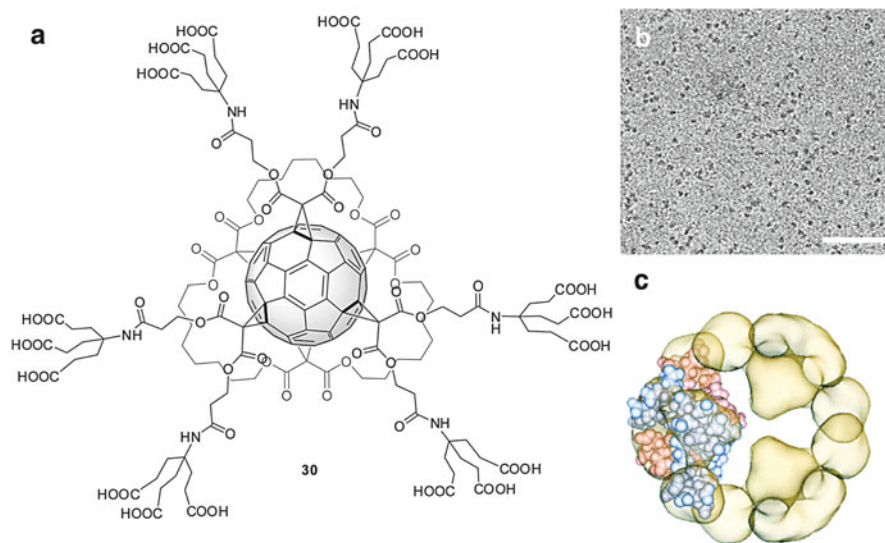
Fig. 23 (**a**) Structure of [3:3]-hexakis C_{60} adduct **30**. (**b**) TEM image of aggregates of **30** using negative-staining technique. The scale bar represents 50 nm. (**c**) 3D reconstruction of the micelle and molecular fitting. Adapted from [86] with permission. Copyright Wiley

self-assemblies of C_{60} amphiphiles but also opened the way for making shape-persistent C_{60}-based micellar superstructures [89]. These results manifested the power of using the "bottom-up" approach to construct controllable and tunable supramolecular structures and nano-devices, such as "nano-containers."

6 Summary and Outlook

The widespread interest in nano-science and technology over the past few decades has greatly inspired and spurred synthetic and material chemists to continually refine their tools to prepare new functional materials with well-defined and control-lable nanoscopic structures. Investigation and exploitation of controlled supramo-lecular self-organization of various C_{60} fullerene derivatives will pave the way for a wide range of applications. However, such undertakings are still facing a number of challenging barriers. The review in this chapter highlights recent progress towards overcoming these challenges. Aggregation of C_{60} amphiphiles tends to take a variety of forms depending on both the properties of the packing molecules and experimental conditions. It is evident that functionalization of C_{60} with rationally designed pendant groups offers an effective approach to avert the random aggrega-tion inherent in spherical C_{60} cage and hence delivers controllability over the microstructure of self-assembly and organization. Yet, the ability to make a priori

prediction on aggregation behaviors and morphological outcomes for various amphiphilic C$_{60}$ building blocks has not been realized. To reach this end, continued efforts to design and synthesize new C$_{60}$ amphiphiles with controlled self-assembly properties and the use of high-resolution analytical techniques to well characterize the nanoscopic details of C$_{60}$ nano-aggregates are imperative and indispensable. Additionally, it is worth noting that a difficulty in applying amphiphilic packing theories to rationalize aggregation outcomes lies in *how to properly describe the molecular shapes of complex C$_{60}$ derivatives*. This appears to be an overlooked territory in the recent literature. In this sense, employment of consistent and reliable modeling methods [90–92] rather than empirical estimation to evaluate the shape of molecule will be of great value for facilitating better understanding of the relationship between molecular structure and aggregation properties.

References

1. Kroto HW, Walton DRM (1993) The fullerenes: new horizons for the chemistry, physics and astrophysics of carbon. Cambridge University Press, Cambridge
2. Guldi DM, Martin N (2002) Fullerenes: from synthesis to optoelectronic properties. Kluwer Academic Publishers, Dordrecht
3. Osawa E (2002) Perspectives of fullerene nanotechnology. Kluwer Academic Publishers, Dordrecht
4. Langa F, Nierengarten JF (2007) Fullerenes: principles and applications. Royal Society of Chemistry, Cambridge
5. Taylor R (1999) Lecture notes on fullerene chemistry: a handbook for chemists. Imperial College Press, London
6. Hirsch A, Brettreich M (2005) Fullerenes: chemistry and reactions. Wiley-VCH, Weinheim
7. Martin N, Altable M, Filippone S, Martin-Domenech A (2007) New reactions in fullerene chemistry. Synlett 20:3077–3095
8. Diederich F, Gomez-Lopez M (1999) Supramolecular fullerene chemistry. Chem Soc Rev 28 (5):263–277
9. Bonifazi D, Enger O, Diederich F (2007) Supramolecular [60]fullerene chemistry on surfaces. Chem Soc Rev 36(2):390–414
10. Hahn U, Cardinali F, Nierengarten JF (2007) Supramolecular chemistry for the self-assembly of fullerene-rich dendrimers. New J Chem 31(7):1128–1138
11. Nakamura E, Isobe H (2003) Functionalized fullerenes in water. The first 10 years of their chemistry, biology, and nanoscience. Acc Chem Res 36(11):807–815
12. Gebeyehu D, Brabec CJ, Padinger F, Fromherz T, Hummelen JC, Badt D, Schindler H, Sariciftci NS (2001) The interplay of efficiency and morphology in photovoltaic devices based on interpenetrating networks of conjugated polymers with fullerenes. Synth Met 118 (1–3):1–9
13. Brabec CJ, Zerza G, Cerullo G, De Silvestri S, Luzzati S, Hummelen JC, Sariciftci NS (2001) Tracing photoinduced electron transfer process in conjugated polymer/fullerene bulk heterojunctions in real time. Chem Phys Lett 340(3–4):232–236
14. Park LY, Munro AM, Ginger DS (2008) Controlling film morphology in conjugated polymer: fullerene blends with surface patterning. J Am Chem Soc 130(47):15916–15926
15. Sivula K, Ball ZT, Watanabe N, Fréchet JMJ (2006) Amphiphilic diblock copolymer compatibilizers and their effect on the morphology and performance of polythiophene: fullerene solar cells. Adv Mater 18(2):206–210

16. Campoy-Quiles M, Ferenczi T, Agostinelli T, Etchegoin PG, Kim Y, Anthopoulos TD, Stavrinou PN, Bradley DDC, Nelson J (2008) Morphology evolution via self-organization and lateral and vertical diffusion in polymer: fullerene solar cell blends. Nat Mater 7(2):158–164

17. Hoppe H, Sariciftci NS (2006) Morphology of polymer/fullerene bulk heterojunction solar cells. J Mater Chem 16(1):45–61

18. Hoppe H, Niggemann M, Winder C, Kraut J, Hiesgen R, Hinsch A, Meissner D, Sariciftci NS (2004) Nanoscale morphology of conjugated polymer/fullerene-based bulk-heterojunction solar cells. Adv Funct Mater 14(10):1005–1011

19. Isobe H, Nakanishi W, Tomita N, Jinno S, Okayama H, Nakamura E (2005) Nonviral gene delivery by tetraamino fullerene. Mol Pharm 3(2):124–134

20. Maeda-Mamiya R, Noiri E, Isobe H, Nakanishi W, Okamoto K, Doi K, Sugaya T, Izumi T, Homma T, Nakamura E (2010) In vivo gene delivery by cationic tetraamino fullerene. Proc Natl Acad Sci USA 107(12):5339–5344

21. Han B, Karim MN (2008) Cytotoxicity of aggregated fullerene C_{60} particles on CHO and MDCK cells. Scanning 30(2):213–220

22. Lyon DY, Alvarez PJJ (2008) Fullerene water suspension (nC_{60}) exerts antibacterial effects via ros-independent protein oxidation. Environ Sci Technol 42(21):8127–8132

23. Lyon DY, Brunet L, Hinkal GW, Wiesner MR, Alvarez PJJ (2008) Antibacterial activity of fullerene water suspensions (nC_{60}) is not due to ros-mediated damage. Nano Lett 8(5):1539–1543

24. Sayes CM, Fortner JD, Guo W, Lyon D, Boyd AM, Ausman KD, Tao YJ, Sitharaman B, Wilson LJ, Hughes JB, West JL, Colvin VL (2004) The differential cytotoxicity of water-soluble fullerenes. Nano Lett 4(10):1881–1887

25. Kadish KM, Ruoff RS (2000) Fullerenes: chemistry, physics, and technology. Wiley, New York

26. Ruoff RS, Tse DS, Malhotra R, Lorents DC (1993) Solubility of fullerene (C_{60}) in a variety of solvents. J Phys Chem 97(13):3379–3383

27. Brant JA, Labille J, Bottero J-Y, Wiesner MR (2006) Characterizing the impact of preparation method on fullerene cluster structure and chemistry. Langmuir 22(8):3878–3885

28. Alargova RG, Deguchi S, Tsujii K (2001) Stable colloidal dispersions of fullerenes in polar organic solvents. J Am Chem Soc 123(43):10460–10467

29. Chen KL, Elimelech M (2006) Aggregation and deposition kinetics of fullerene (C_{60}) nanoparticles. Langmuir 22(26):10994–11001

30. Ariga K, Nakanishi T, Hill JP (2007) Self-assembled microstructures of functional molecules. Curr Opin Coll Inter Sci 12(3):106–120

31. Shimizu T, Masuda M, Minamikawa H (2005) Supramolecular nanotube architectures based on amphiphilic molecules. Chem Rev 105(4):1401–1444

32. Hoeben FJM, Jonkheijm P, Meijer EW, Schenning APHJ (2005) About supramolecular assemblies of π-conjugated systems. Chem Rev 105(4):1491–1546

33. Chandler D (2005) Interfaces and the driving force of hydrophobic assembly. Nature 437 (7059):640–647

34. Tsonchev S, Schatz GC, Ratner MA (2003) Hydrophobically-driven self-assembly: a geometric packing analysis. Nano Lett 3(5):623–626

35. Tsonchev S, Troisi A, Schatz GC, Ratner MA (2004) On the structure and stability of self-assembled zwitterionic peptide amphiphiles: a theoretical study. Nano Lett 4(3):427–431

36. Tsonchev S, Troisi A, Schatz GC, Ratner MA (2004) All-atom numerical studies of self-assembly of zwitterionic peptide amphiphiles. J Phys Chem B 108(39):15278–15284

37. Tsonchev S, Schatz GC, Ratner MA (2004) Electrostatically-directed self-assembly of cylindrical peptide amphiphile nanostructures. J Phys Chem B 108(26):8817–8822

38. Velichko YS, Stupp SI, de la Cruz MO (2008) Molecular simulation study of peptide amphiphile self-assembly. J Phys Chem B 112(8):2326–2334

39. Guldi DM, Zerbetto F, Georgakilas V, Prato M (2005) Ordering fullerene materials at nanometer dimensions. Acc Chem Res 38(1):38–43
40. Cassell AM, Asplund CL, Tour JM (1999) Self-assembling supramolecular nanostructures from a C_{60} derivative: nanorods and vesicles. Angew Chem Int Ed 38(16):2403–2405
41. Nakashima N, Ishii T, Shirakusa M, Nakanishi T, Murakami H, Sagara T (2001) Molecular bilayer-based superstructures of a fullerene-carrying ammonium amphiphile: structure and electrochemistry. Chem Eur J 7(8):1766–1772
42. Georgakilas V, Pellarini F, Prato M, Guldi DM, Melle-Franco M, Zerbetto F (2002) Supramolecular self-assembled fullerene nanostructures. Proc Natl Acad Sci USA 99(8):5075–5080
43. Angelini G, De Maria P, Fontana A, Pierini M, Maggini M, Gasparrini F, Zappia G (2001) Study of the aggregation properties of a novel amphiphilic C_{60} fullerene derivative. Langmuir 17(21):6404–6407
44. Brough P, Bonifazi D, Prato M (2006) Self-organization of amphiphilic [60]fullerene derivatives in nanorod-like morphologies. Tetrahedron 62(9):2110–2114
45. Fuhrhop J-H, Wang T (2004) Bolaamphiphiles. Chem Rev 104(6):2901–2938
46. Sano M, Oishi K, Ishi-i T, Shinkai S (2000) Vesicle formation and its fractal distribution by bola-amphiphilic [60]fullerene. Langmuir 16(8):3773–3776
47. Guldi DM, Gouloumis A, Vázquez P, Torres T, Georgakilas V, Prato M (2005) Nanoscale organization of a phthalocyanine−fullerene system: remarkable stabilization of charges in photoactive 1-d nanotubules. J Am Chem Soc 127(16):5811–5813
48. Angelini G, Cusan C, De Maria P, Fontana A, Maggini M, Pierini M, Prato M, Schergna S, Villani C (2005) The associative properties of some amphiphilic fullerene derivatives. Eur J Org Chem 2005(9):1884–1891
49. Guldi DM, Maggini M, Mondini S, Guérin F, Fendler JH (1999) Formation, characterization, and properties of nanostructured $[Ru(bpy)_3]^{2+}$-C_{60} langmuir−blodgett films in situ at the air−water interface and ex situ on substrates. Langmuir 16(3):1311–1318
50. Guldi DM, Luo C, Koktysh D, Kotov NA, Da Ros T, Bosi S, Prato M (2002) Photoactive nanowires in fullerene−ferrocene dyad polyelectrolyte multilayers. Nano Lett 2(7):775–780
51. Chuard T, Deschenaux R (1996) First fullerene[60]-containing thermotropic liquid crystal. Preliminary communication. Helv Chim Acta 79(3):736–741
52. Murakami H, Watanabe Y, Nakashima N (1996) Fullerene lipid chemistry: self-organized multibilayer films of a C_{60}-bearing lipid with main and subphase transitions. J Am Chem Soc 118(18):4484–4485
53. Chuard T, Deschenaux R (2002) Design, mesomorphic properties, and supramolecular organization of [60]fullerene-containing thermotropic liquid crystals J Mater Chem 12:1944–1951
54. Lenoble J, Campidelli S, Maringa N, Donnio B, Guillon D, Yevlampieva N, Deschenaux R (2007) Liquid−crystalline janus-type fullerodendrimers displaying tunable smectic−columnar mesomorphism. J Am Chem Soc 129(32):9941–9952
55. Li W-S, Yamamoto Y, Fukushima T, Saeki A, Seki S, Tagawa S, Masunaga H, Sasaki S, Takata M, Aida T (2008) Amphiphilic molecular design as a rational strategy for tailoring bicontinuous electron donor and acceptor arrays: photoconductive liquid crystalline oligothiophene−C_{60} dyads. J Am Chem Soc 130(28):8886–8887
56. Campidelli S, Bourgun P, Guintchin B, Furrer J, Stoeckli-Evans H, Saez IM, Goodby JW, Deschenaux R (2010) Diastereoisomerically pure fulleropyrrolidines as chiral platforms for the design of optically active liquid crystals. J Am Chem Soc 132(10):3574–3581
57. Nakanishi T, Schmitt W, Michinobu T, Kurth DG, Ariga K (2005) Hierarchical supramolecular fullerene architectures with controlled dimensionality. Chem Commun 5982–5984
58. Nakanishi T, Ariga K, Michinobu T, Yoshida K, Takahashi H, Teranishi T, Möhwald H, Kurth DG (2007) Flower-shaped supramolecular assemblies: hierarchical organization of a fullerene bearing long aliphatic chains. Small 3(12):2019–2023
59. Nakanishi T, Michinobu T, Yoshida K, Shirahata N, Ariga K, Möhwald H, Kurth DG (2008) Nanocarbon superhydrophobic surfaces created from fullerene-based hierarchical supramolecular assemblies. Adv Mater 20(3):443–446

60. Shen Y, Skirtach AG, Seki T, Yagai S, Li H, Möhwald H, Nakanishi T (2010) Assembly of fullerene-carbon nanotubes: temperature indicator for photothermal conversion. J Am Chem Soc 132 (25):8566–8568
61. Tomalia DA (2010) Dendrons/dendrimers: quantized, nano-element like building blocks for soft-soft and soft-hard nano-compound synthesis. Soft Matter 6:456–474
62. Fréchet JMJ, Tomalia DA (2001) Dendrimers and other dendritic polymers. Wiley, Chichester
63. Newkome GR, Moorefield CN, Vögtle F (2001) Dendrimers and dendrons: concepts, syntheses, applications. Wiley-VCH, Weinheim
64. Rosen BM, Wilson CJ, Wilson DA, Peterca M, Imam MR, Percec V (2009) Dendron-mediated self-assembly, disassembly, and self-organization of complex systems. Chem Rev 109 (11):6275–6540
65. Nierengarten J-F (2000) Fullerodendrimers: a new class of compounds for supramolecular chemistry and materials science applications. Chem Eur J 6(20):3667–3670
66. Nierengarten JF (2004) Chemical modification of C_{60} for materials science applications. New J Chem 28:1177–1191
67. Arai T, Ogawa J, Mouri E, Bhuiyan MPI, Nishino N (2006) Formation of submicron scale particles of narrow size distribution from a water-soluble dendrimer with links to porphyrins and a fullerene. Macromolecules 39(4):1607–1613
68. Fernández G, Pérez EM, Sánchez L, Martín N (2008) An electroactive dynamically polydisperse supramolecular dendrimer. J Am Chem Soc 130(8):2410–2411
69. Mahmud IM, Zhou N, Wang L, Zhao Y (2008) Triazole-linked dendro[60]fullerenes: modular synthesis via a "click" reaction and acidity-dependent self-assembly on the surface. Tetrahedron 64(50):11420–11432
70. Matsuo Y, Muramatsu A, Hamasaki R, Mizoshita N, Kato T, Nakamura E (2003) Stacking of molecules possessing a fullerene apex and a cup-shaped cavity connected by a silicon connection. J Am Chem Soc 126(2):432–433
71. Kato H, Böttcher C, Hirsch A (2007) Sugar balls: Synthesis and supramolecular assembly of [60]fullerene glycoconjugates. Eur J Org Chem 16:2659–2666
72. Liu B, Yang M, Zhang Z, Zhang G, Han Y, Xia N, Hu M, Zheng P, Wang W (2010) Ribbonlike assembly of molecules composed of fulleropyrrolidine and PUA dendron. Langmuir 26 (12):9403–9407
73. Sawamura M, Iikura H, Nakamura E (1996) The first pentahaptofullerene metal complexes. J Am Chem Soc 118(50):12850–12851
74. Zhong Y-W, Matsuo Y, Nakamura E (2006) Convergent synthesis of a polyfunctionalized fullerene by regioselective five-fold addition of a functionalized organocopper reagent to C_{60}. Org Lett 8(7):1463–1466
75. Sawamura M, Nagahama N, Toganoh M, Nakamura E (2002) Regioselective penta-addition of 1-alkenyl copper reagent to [60]fullerene. Synthesis of penta-alkenyl FCp ligand. J Organomet Chem 652(1–2):31–35
76. Sawamura M, Nagahama N, Toganoh M, Hackler UE, Isobe H, Nakamura E, Zhou S-Q, Chu B (2000) Pentaorgano[60]fullerene $R_5C_{60}^-$. A water soluble hydrocarbon anion. Chem Lett 1098–1099
77. Zhou S, Burger C, Chu B, Sawamura M, Nagahama N, Toganoh M, Hackler UE, Isobe H, Nakamura E (2001) Spherical bilayer vesicles of fullerene-based surfactants in water: a laser light scattering study. Science 291(5510):1944–1947
78. Homma T, Harano K, Isobe H, Nakamura E (2010) Nanometer-sized fluorous fullerene vesicles in water and on solid surfaces. Angew Chem Int Ed 49:1665–1668
79. Burger C, Hao J, Ying Q, Isobe H, Sawamura M, Nakamura E, Chu B (2004) Multilayer vesicles and vesicle clusters formed by the fullerene-based surfactant $C_{60}(CH_3)_5K$. J Colloid Interface Sci 275(2):632–641
80. Cardullo F, Diederich F, Echegoyen L, Habicher T, Jayaraman N, Leblanc RM, Stoddart JF, Wang S (1998) Stable langmuir and langmuir−blodgett films of fullerene−glycodendron conjugates. Langmuir 14(8):1955–1959

81. Felder D, del Pilar Carreon M, Gallani J-L, Guillon D, Nierengarten J-F, Chuard T, Deschenaux R (2001) Amphiphilic fullerene-cholesterol derivatives: synthesis and preparation of Langmuir and Langmuir–Blodgett films. Helv Chim Acta 84(5):1119–1132
82. Felder D, Gutierrez Nava M, del Pilar Carreon M, Eckert J-F, Luccisano M, Schall C, Masson P, Gallani J-L, Heinrich B, Guillon D, Nierengarten J-F (2002) Synthesis of amphiphilic fullerene derivatives and their incorporation in Langmuir and Langmuir–Blodgett films. Helv Chim Acta 85(1):288–319
83. Zhang S, Rio Y, Cardinali F, Bourgogne C, Gallani J-L, Nierengarten J-F (2003) Amphiphilic diblock dendrimers with a fullerene core. J Org Chem 68(25):9787–9797
84. Felder-Flesch D, Bourgogne C, Gallani J-L, Guillon D (2005) Interfacial behavior and film-forming properties of an amphiphilic hexasubstituted [60]fullerene. Tetrahedron Lett 46 (38):6507–6510
85. Maierhofer AP, Brettreich M, Burghardt S, Vostrowsky O, Hirsch A, Langridge S, Bayerl TM (2000) Structure and electrostatic interaction properties of monolayers of amphiphilic molecules derived from C$_{60}$-fullerenes: a film balance, neutron-, and infrared reflection study. Langmuir 16(23):8884–8891
86. Burghardt S, Hirsch A, Schade B, Ludwig K, Böttcher C (2005) Switchable supramolecular organization of structurally defined micelles based on an amphiphilic fullerene. Angew Chem Int Ed 44(19):2976–2979
87. Brettreich M, Burghardt S, Böttcher C, Bayerl T, Bayerl S, Hirsch A (2000) Globular amphiphiles: membrane-forming hexaadducts of C$_{60}$. Angew Chem Int Ed 39(10):1845–1848
88. Schade B, Ludwig K, Böttcher C, Hartnagel U, Hirsch A (2007) Supramolecular structure of 5-nm spherical micelles with D_3 symmetry assembled from amphiphilic [3:3]-hexakis adducts of C$_{60}$. Angew Chem Int Ed 46(23):4393–4396
89. Hirsch A (2008) Amphiphilic architectures based on fullerene and calixarene platforms: from buckysome to shape-persistent micelles. Pure Appl Chem 80(3):571–587
90. Grant JA, Gallardo MA, Pickup BT (1996) A fast method of molecular shape comparison: a simple application of a gaussian description of molecular shape. J Comput Chem 17 (14):1653–1666
91. Grant JA, Pickup BT, Sykes MJ, Kitchen CA, Nicholls A (2007) The gaussian generalized born model: application to small molecules. Phys Chem Chem Phys 9(35):4913–4922
92. Gong LD, Yang ZZ (2010) Investigation of the molecular surface area and volume: defined and calculated by the molecular face theory. J Comput Chem 31(11):2098–2108